Role of the plasmon-pole model in the *GW* approximation

Paul Larson, Marc Dvorak, and Zhigang Wu*
Department of Physics, Colorado School of Mines, Golden, Colorado 80401, USA
(Received 14 June 2013; revised manuscript received 29 August 2013; published 10 September 2013)

Band gaps and band-edge energy levels are computed using the many-body perturbation theory within the *GW* approximation, with four common plasmon pole models (PPMs) and numerical integration employed to evaluate the dynamic screening matrix. Although the Hybertsen-Louie PPM is often adopted in *GW* calculations because it predicts band gaps best matching experimental data, we show that it is the Godby-Needs construction that agrees consistently with numerical integration on dynamic screening for materials with distinct characteristics. The variation in predicted band gaps due to different PPMs used can be as large as 1 eV in strongly localized electronic systems, and the band-edge energy levels are more sensitive to the choice of PPM than band gap even in simple semiconductors.

DOI: 10.1103/PhysRevB.88.125205 PACS number(s): 71.15.Mb, 71.15.Qe, 71.20.Nr

I. INTRODUCTION

Density functional theory (DFT)[1,2] calculations employing simple exchange-correlation functionals, such as the local density approximation (LDA) and the generalized gradient approximation (GGA), severely underestimate the fundamental band gaps, E_g, of semiconductors and insulators[3–6] due to the lack of derivative discontinuity with respect to the number of electrons.[7–9] While the orbital-dependent density functionals,[10,11] such as the hybrid functionals,[12–14] could significantly improve electronic-structure calculations, their accuracy depends on parametrization and varies among different materials.

The standard method for obtaining the quasiparticle (QP) energies is based on the single-particle Green function G and the self-energy Σ within the framework of the many-body perturbation theory.[15,16] A practical and successful scheme for quantitatively computing self-energy is the *GW* approximation,[3–6] in which Σ is approximated by the linear expansion of G and the dynamically screened Coulomb interaction W, symbolically designated as

$$\Sigma = iGW. \tag{1}$$

Self-consistent *GW* calculations[17–21] are extremely demanding. In practice, the single-shot G_0W_0 (Refs. 3,22, and 23) has been widely adopted, since it offers sufficient accuracy on E_g for many crystals including simple semiconductors and insulators. However, different levels of self-consistency (such as G_0W_0, GW_0, and GW) in *GW* calculations might change E_g as much as 1 eV in some transition-metal oxides.[20,24–26] Furthermore, the plasmon-pole approximation[4,5,27–30] is commonly made to efficiently obtain the dynamic screening. Many plasmon-pole models (PPMs)[3,31–34] based on different considerations have been constructed, and most *GW* calculations were carried out by simply choosing one PPM that best reproduces the experimental data of band gaps. Moreover, pseudopotentials and the treatment of the semicore states[4,5,20,25,35–37] could also have major impacts on electronic band structures. Thus, the true performance of the *GW* approximation is *obscured* by these additional approximations, which need to be investigated separately in order to systematically assess and then improve the *GW* method.

In this work, we carry out G_0W_0 calculations on a variety of materials. To single out the effects of the PPM, we compare our results using four usual PPMs with those obtained by numerical integration of dynamic screening, instead of experimental data. For systems with highly localized valence electrons the predicted E_g can vary as much as 1 eV using different PPMs, while for strongly delocalized electronic systems E_g barely changes with respect to the numerical integration results; however, the energies of the band-edge states are much more sensitive to the choice of PPM. Our calculations and analysis suggest that the simplest PPM satisfying no f-sum rules, i.e., the Godby-Needs model,[31,32] best describes the dynamic screening.

II. METHOD

Calculations were performed using the ABINIT package.[38] Convergences on the size of the reciprocal mesh, the cutoff energies, and the number of conduction bands were carefully examined, so that a $6 \times 6 \times 6$ **k** mesh was used for C and Si while a $4 \times 4 \times 4$ **k** mesh was found large enough for the remaining materials we studied, and cutoff energies up to 80 Ry were used. Norm-conserving pseudopotentials are employed; in particular, the Zn semicore states $3s$, $3p$, and $3d$ are treated as valence states. The number of conduction bands used to evaluate electronic screening vary from about 200 for Si to over 2000 for ZnO, and four PPMs, namely Godby-Needs (GN),[31,32] Hybertsen-Louie (HL),[3] von der Linden–Horsch (vdLH),[33] and Engel-Farid (EF),[34] together with numerical integration, were employed. The contour numerical integration method for obtaining self-energy is described in detail in Refs. 39 and 40; because the integrand is quite smooth, 12–20 frequencies in a range from 0 to 30–60 eV along both axes are found sufficient to obtain well-converged results for these materials.

III. RESULTS AND DISCUSSION

Table I summarizes the calculated E_g of materials ranging from simple semiconductors and insulators to transition-metal oxide ZnO and molecular solid noble gas Ne. Compared with experimental data corrected by excluding the electron-phonon interactions,[41] which normally lead to a reduced band gap,[42–46] E_g in AlN, GaAs, ZnO, and Ne have relatively large errors,

TABLE I. Calculated G_0W_0 band gaps (in eV) using the four plasmon-pole models of GN, HL, vdLH, and EF, compared to numerical integration and experimental data, which exclude the electron-phonon interaction. The last column reports the invariant part of the localization length ($\sigma_{\rm el}^{\rm inv}$) of valence electrons.

	GN	HL	vdLH	EF	Numerical	Expt.	$\sigma_{\rm el}^{\rm inv}$ (Å)
Si	1.20	1.25	1.23	1.26	1.21	1.24	1.465
C	6.10	6.25	6.25	6.29	6.15	6.11	0.838
Ge	0.68	0.72	0.70	0.71	0.69	0.85	1.533
Ne	19.65	20.99	20.51	19.99	19.41	21.50	0.879
AlN	5.55	5.73	5.71	5.74	5.59	6.29	0.891
GaN	3.51	3.61	3.62	3.66	3.54	3.44	1.064
GaAs	1.13	1.15	1.14	1.16	1.13	1.59	1.527
MgO	7.13	7.61	7.46	7.39	7.13	7.85	0.838
ZnO	2.27	2.80	2.30	2.37	2.17	3.53	0.920

requiring self-consistent GW computations[19,20] and/or more accurate DFT wave functions to construct G and W.[37,47–50] Here we focus on the effects of the PPM on band structures, and our calculations suggest that for Si, Ge, and GaAs all four PPMs give very close $E_{\rm g}$ values (within 0.1 eV) to those from numerical integration. For AlN, GaN, and C, variations in $E_{\rm g}$ are in the range 0.1–0.2 eV, while for MgO, ZnO, and Ne the differences in $E_{\rm g}$ are larger than 0.5 eV using various PPMs. For all these materials the GN PPM always agrees very well with the numerical integration, whereas the other three PPMs tend to overestimate $E_{\rm g}$, which is especially significant in MgO, ZnO, and Ne.

We also studied the effects of the PPM on the many-body corrections to individual QP energies, as summarized in Table II for the conduction-band minimum (CBM) and valence-band maximum (VBM). Although the variations in $\Delta E_{\rm g}$ ($E_{\rm g}^{G_0W_0} - E_{\rm g}^{\rm DFT}$) of Si and C are negligible using these four PPMs, the many-body corrections to CBM (ΔE_c) and VBM (ΔE_v) vary noticeably. We find that (1) the GN results are very different from the HL, vdLH, and EF results, which are relatively similar; (2) for solid Ne, ΔE_c is not sensitive to the choice of PPM, while ΔE_v depends strongly on the PPM;

TABLE II. Calculated G_0W_0 corrections (in eV) to DFT CBM (ΔE_c), VBM (ΔE_v), and band gaps ($\Delta E_{\rm g}$) using the four plasmon-pole models of GN, HL, vdLH, and EF, compared to numerical integration.

		GN	HL	vdLH	EF	Numerical
Si	ΔE_c	0.50	0.22	0.21	0.26	0.51
	ΔE_v	−0.15	−0.48	−0.47	−0.45	−0.11
	$\Delta E_{\rm g}$	0.65	0.70	0.68	0.71	0.62
C	ΔE_v	1.16	0.77	0.75	0.82	1.09
	ΔE_c	−0.19	−0.73	−0.75	−0.72	−0.30
	$\Delta E_{\rm g}$	1.35	1.50	1.50	1.54	1.39
Ne	ΔE_c	2.80	2.67	2.69	2.74	2.84
	ΔE_v	−5.48	−6.95	−6.45	−5.88	−5.20
	$\Delta E_{\rm g}$	8.28	9.62	9.14	8.62	8.04
ZnO	ΔE_c	0.79	0.13	0.22	0.51	0.78
	ΔE_v	−0.61	−1.80	−1.21	−0.99	−0.52
	$\Delta E_{\rm g}$	1.40	1.93	1.43	1.50	1.30

(3) both ΔE_c and ΔE_v for ZnO change considerably when varying the PPM; and (4) for all these materials the GN results of ΔE_c and ΔE_v agree excellently with those from numerical integration, which is consistent with the previous work.[51]

Since the PPM approximates the dynamic screening, which is strongly correlated to the level of electron delocalization,[52,53] we quantify this by computing the localization length ($\sigma_{\rm el}$) of valence electrons. Here $\sigma_{\rm el} = \sqrt{S}/N$, and the spread functional S of an N-band crystal in real space is defined as

$$S = \sum_{n=1}^{N} \left[\langle r^2 \rangle_n - \langle \mathbf{r} \rangle_n^2 \right]. \tag{2}$$

S can be decomposed into one gauge-invariant term $S^{\rm inv}$ and a variant term $\tilde{S}$, and the minimized $\tilde{S}$ can be obtained by employing the WANNIER90 code[52,54] to search over a range of unitary transformations to the wave functions.

The last column of Table I shows the calculated invariant part of the localization lengths $\sigma_{\rm el}^{\rm inv}$, which clearly suggests that for the highly delocalized electronic systems, such as Si, Ge, and GaAs, these four PPMs behave very similarly to numerical integration on band gaps, whereas for the strongly localized systems such as MgO, ZnO, and Ne, the G_0W_0 band gaps differ significantly with different PPMs used, as visualized in Fig. 1. We note that although C has a $\sigma_{\rm el}^{\rm inv}$ comparable to those of ZnO and Ne, its lattice constant is much smaller than those of ZnO, Ne, and Si; therefore, its valence electrons are much less localized than ZnO and Ne, as graphically demonstrated in Fig. 2: ZnO and Ne have strongly localized valence electron distributions, whereas the valence electrons in Si and C are much more extended.

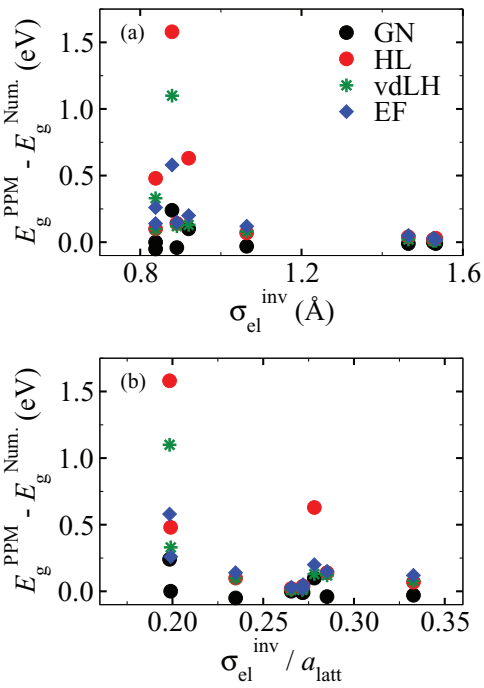

FIG. 1. (Color online) Performance of four PPMs on band gap ($E_{\rm g}$) with respect to localization length (σ) of valence electrons. Here the vertical axes are the difference in computed $E_{\rm g}$ using PPMs and numerical integration; (a) the horizontal axis is the invariant part of the localization length, and (b) it is scaled by lattice constant $a_{\rm latt}$.

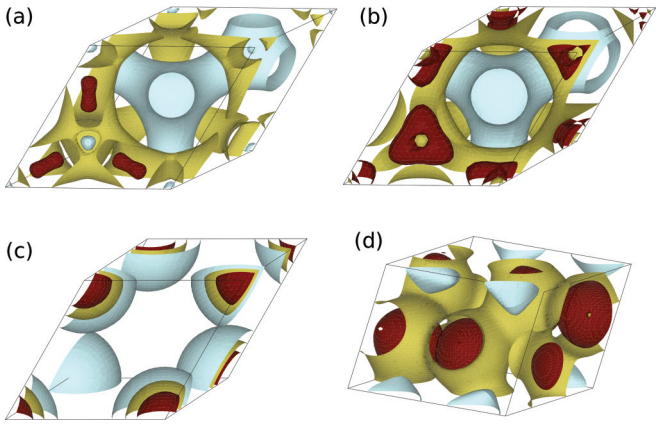

FIG. 2. (Color online) Isosurfaces of the valence charge densities for (a) Si, (b) C, (c) Ne, and (d) ZnO. Here four valence bands for Si, C, and Ne and six for ZnO are included, and the corresponding isosurface values are set to be identical in four panels, with high to low values ranging from red (dark) to yellow (light) colors.

To understand why the performances of these PPMs compared with numerical integration depend on the electron delocalization level, we briefly describe how these PPMs were constructed. In the GW approximation, self-energy Σ is the product of the QP Green function G and the screened Coulomb interaction

$$W = \varepsilon^{-1} V, \tag{3}$$

where ε is the dielectric response function and V the bare Coulomb interaction. Evaluation of $\varepsilon^{-1}(\mathbf{r},\mathbf{r}',\omega)$, or its Fourier transformation in the reciprocal space, $\varepsilon^{-1}_{\mathbf{G},\mathbf{G}'}(\mathbf{q},\omega)$, with $\mathbf{G}$ and $\mathbf{G}'$ the reciprocal lattice vectors and $\mathbf{q}$ a wave vector in the first Brillouin zone, remains a major numerical challenge due to spatial nonlocality and frequency (ω) dependence. The plasmon-pole approximation takes advantage of the fact that ε^{-1} is usually flat except for a peak at the plasma frequency, ω_p, assuming that reproducing the actual shape of ε^{-1} is less important than reproducing the convolution of G and W in the frequency space. Thus $\varepsilon^{-1}_{\mathbf{G},\mathbf{G}'}(\mathbf{q},\omega)$ can be approximated by a single-pole function in ω, with the effective strength and frequency of the plasmon excitation modeled by imposing certain constraints and/or exact values and limits, such as the static dielectric function.

The earliest PPM[15] was simply a Dirac δ function for a homogenous electron gas, which can replicate the major features of the GW integral fairly well. The GN PPM,[31,32] constructed by fitting $\varepsilon^{-1}_{\mathbf{G},\mathbf{G}'}(\mathbf{q},\omega)$ at two points along the imaginary frequency axis, is little more than the Dirac δ-function solution with a rapidly decaying tail. On the contrary, the HL,[3] vdLH,[33] and EF[34] models use the zero-frequency limit and the f-sum rule analogous to Johnson's formalism[55,56] to fix their parameters.

Specifically, in the GN and HL PPMs, the Kramers-Kronig relation between the real and imaginary parts of ε^{-1} is enforced, so that

$$\mathrm{Im}\left[\varepsilon^{-1}_{\mathbf{G},\mathbf{G}'}(\mathbf{q},\omega)\right] = A_{\mathbf{G},\mathbf{G}'}(\mathbf{q})\,[\delta(\omega-\tilde{\omega}_{\mathbf{G},\mathbf{G}'}(\mathbf{q})) - \delta(\omega+\tilde{\omega}_{\mathbf{G},\mathbf{G}'}(\mathbf{q}))], \tag{4a}$$

$$\mathrm{Re}\left[\varepsilon^{-1}_{\mathbf{G},\mathbf{G}'}(\mathbf{q},\omega)\right] = \delta_{\mathbf{G},\mathbf{G}'} + \frac{\Omega^2_{\mathbf{G},\mathbf{G}'}(\mathbf{q})}{\omega^2 - \tilde{\omega}^2_{\mathbf{G},\mathbf{G}'}(\mathbf{q})}. \tag{4b}$$

Here $\tilde{\omega}_{\mathbf{G},\mathbf{G}'}(\mathbf{q})$ is the plasmon frequency with effective strength amplitude $A_{\mathbf{G},\mathbf{G}'}(\mathbf{q})$, and $\Omega^2_{\mathbf{G},\mathbf{G}'}(\mathbf{q}) = -A_{\mathbf{G},\mathbf{G}'}(\mathbf{q})\tilde{\omega}^2_{\mathbf{G},\mathbf{G}'}(\mathbf{q})$. The GN PPM reproduces $\varepsilon^{-1}_{\mathbf{G},\mathbf{G}'}(\mathbf{q},\omega)$ at $\omega \to 0$ and $\omega \to i\omega_p$, while Hybertsen and Louie imposed a generalized f-sum rule,

$$\int_0^\infty d\omega\,\omega\,\mathrm{Im}\left[\varepsilon^{-1}_{\mathbf{G},\mathbf{G}'}(\mathbf{q},\omega)\right] = -\frac{\pi}{2}\omega_p^2\,\frac{(\mathbf{q}+\mathbf{G})\cdot(\mathbf{q}+\mathbf{G}')}{|\mathbf{q}+\mathbf{G}|^2}\,\frac{\rho(\mathbf{G}-\mathbf{G}')}{\rho(0)}, \tag{5}$$

where ρ is the electron density. In the HL construction the off-diagonal dielectric matrix elements are unphysical, and it is nontrivial to generalize the HL model to systems without inversion symmetry.[57] The vdLH and EF PPMs improve the off-diagonal matrix elements over the HL PPM. The vdLH model[33] adds the frequency dependence to the eigenvalues of the dielectric matrix ε^{-1}, making the off-diagonal elements physically meaningful, whereas the EF[34] PPM introduces frequency dependence to both the eigenvalues and the eigenvectors of inverse polarizability χ^{-1}, and the χ^{-1} matrices are diagonalized in the limits of $\omega \to 0$ and $\omega \to \infty$, so that the f-sum rule is followed.

We analyze the properties of the dielectric functions obtained using the plasmon-pole approximation, in comparison with those obtained by numerical integration. Figures 3 and 4 plot $\mathrm{Re}[\varepsilon^{-1}(\mathbf{q}=0,\omega)]$ along the imaginary and real frequency axes, respectively, for $\mathbf{G}=\mathbf{G}'=0$, the Brillouin zone center. The results for the GN and HL PPMs are shown for four representative materials, Si, C, ZnO, and Ne; since the HL, vdLH, and EF PPMs were all constructed by enforcing the f-sum rule, here we only discuss the GN and HL PPMs, expecting the vdLH and EF PPMs to behave somewhat similarly to the HL PPM.

Figure 3(a) indicates that for Si the GN and HL PPMs both reproduce the actual $\mathrm{Re}[\varepsilon^{-1}]$ at $\mathbf{G}=\mathbf{G}'=0$ along the imaginary ω axis very well. This is because both models become exact for the homogeneous electron gas, and the screening of highly delocalized valence electrons in materials such as simple semiconductors can be approximated by a uniform gas locally, which is analogous to the local density approximation for the exchange-correlation functional. For C, the GN PPM also reproduces the actual $\mathrm{Re}[\varepsilon^{-1}(i\omega)]$ very well, while the HL PPM is less accurate, underestimating $\mathrm{Re}[\varepsilon^{-1}(i\omega)]$ noticeably, as shown in Fig. 3(b). This is in line with the fact that the valence electrons in C are less delocalized than those in Si. In contrast, Figs. 3(c) and 3(d) indicate that in Ne and ZnO, where the valence electrons are strongly localized [Figs. 2(c) and 2(d)], values of $\mathrm{Re}[\varepsilon^{-1}(i\omega)]$ computed by the HL PPM are significantly lower than the actual values, while the GN PPM still makes good matches to the numerical results of $\mathrm{Re}[\varepsilon^{-1}(i\omega)]$.

The same trend holds for $\mathrm{Re}[\varepsilon^{-1}]$ at $\mathbf{G}=\mathbf{G}'=0$ along the real ω axis. Figure 4 demonstrates that for Si and C, the GN and HL PPMs both can well reproduce the actual values of $\mathrm{Re}[\varepsilon^{-1}(\omega)]$, except for the region near the plasma frequency ω_p, while for Ne and ZnO both models are too crude to capture the fine features of $\mathrm{Re}[\varepsilon^{-1}(i\omega)]$ over a broad

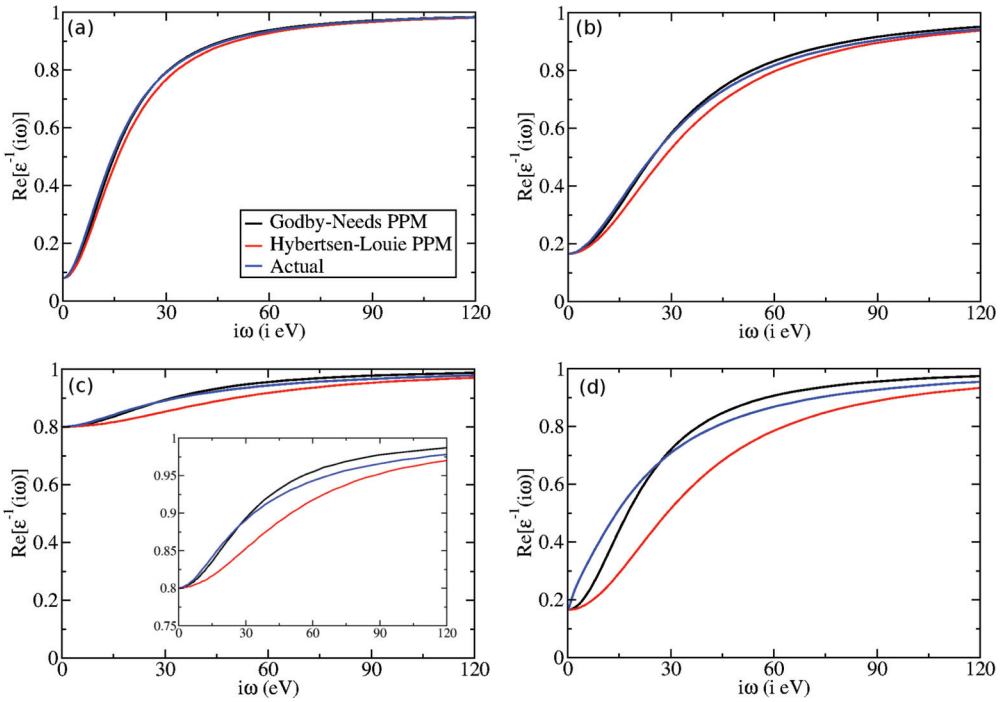

FIG. 3. (Color online) The real part of the inverse dielectric function at $\mathbf{G} = \mathbf{G}' = 0$ along the imaginary frequency axis for (a) Si, (b) C, (c) Ne, and (d) ZnO, using the GN and HL PPMs, compared to those obtained by numerical integration.

region centered about the plasma frequency. However, even in strongly localized electronic systems such as Ne and ZnO, the GN model is still better than the HL model in that the HL PPM *overestimates* the plasma frequency due to enforcing the f-sum rule, whereas the GN PPM asserts the actual plasmon pole positions.

We also computed values of $\mathrm{Re}[\varepsilon^{-1}]$ at $\mathbf{G}$ and $\mathbf{G}'$ other than the Γ point, which are plotted in Figs. 5 and 6 and show the similar trend is also revealed. Thus our calculations demonstrate that in highly delocalized electronic systems such as Si and C, the GN and HL PPMs (together with the vdLH and EF PPMs) behave similarly; however, in strongly localized

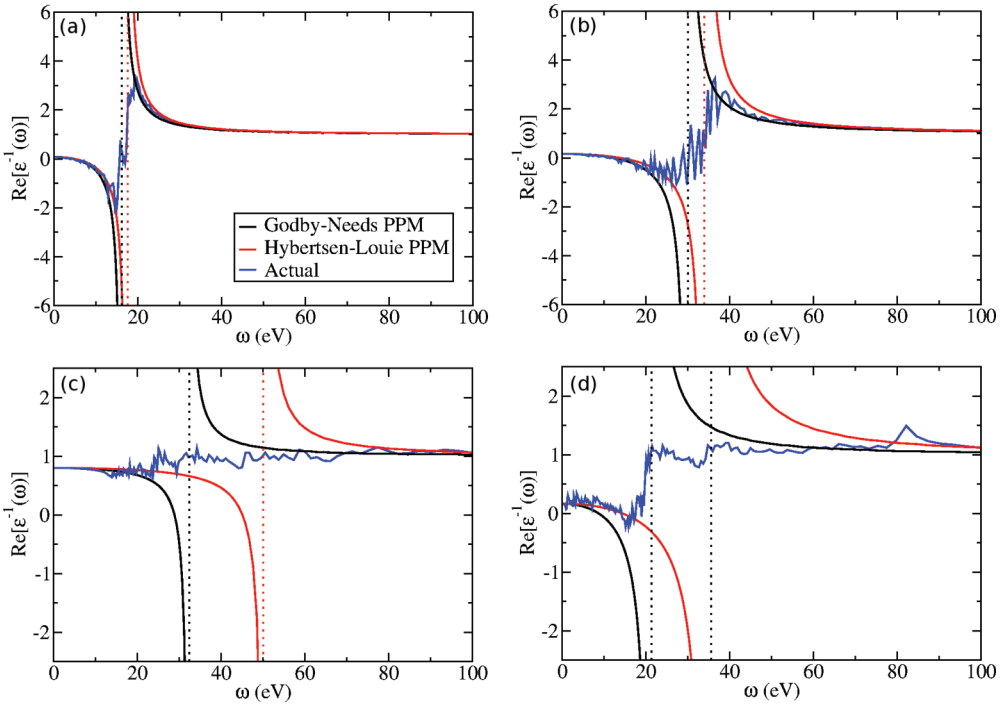

FIG. 4. (Color online) The real part of the inverse dielectric function at $\mathbf{G} = \mathbf{G}' = 0$ along the real frequency axis for (a) Si, (b) C, (c) Ne, and (d) ZnO, using the GN and HL PPMs, compared to those obtained by numerical integration.

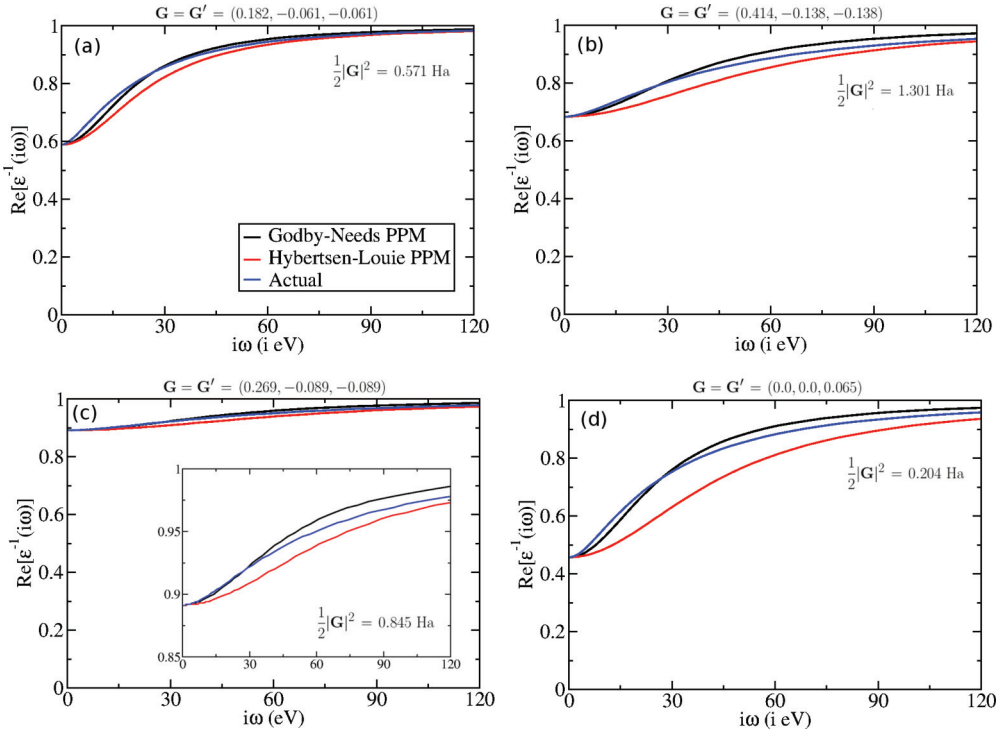

FIG. 5. (Color online) The real part of the inverse dielectric function along the imaginary frequency axis for (a) Si, (b) C, (c) Ne, and (d) ZnO, using the GN and HL PPMs, compared to those obtained from numerical integration. Here $\mathbf{G} = \mathbf{G}' \neq 0$.

electronic systems such as Ne and ZnO, the GN and HL PPMs differ notably, and the choice of PPM greatly affects the magnitude of E_g. Although E_g obtained using the HL PPM in general best agrees with experimental data among these PPMs, especially for strongly localized electron systems, it is the GN PPM that can predict E_g more accurately than the other three PPMs, compared with the numerical integration results.

The HL PPM tends to underestimate screening and thus exaggerate the many-body corrections to the Kohn-Sham

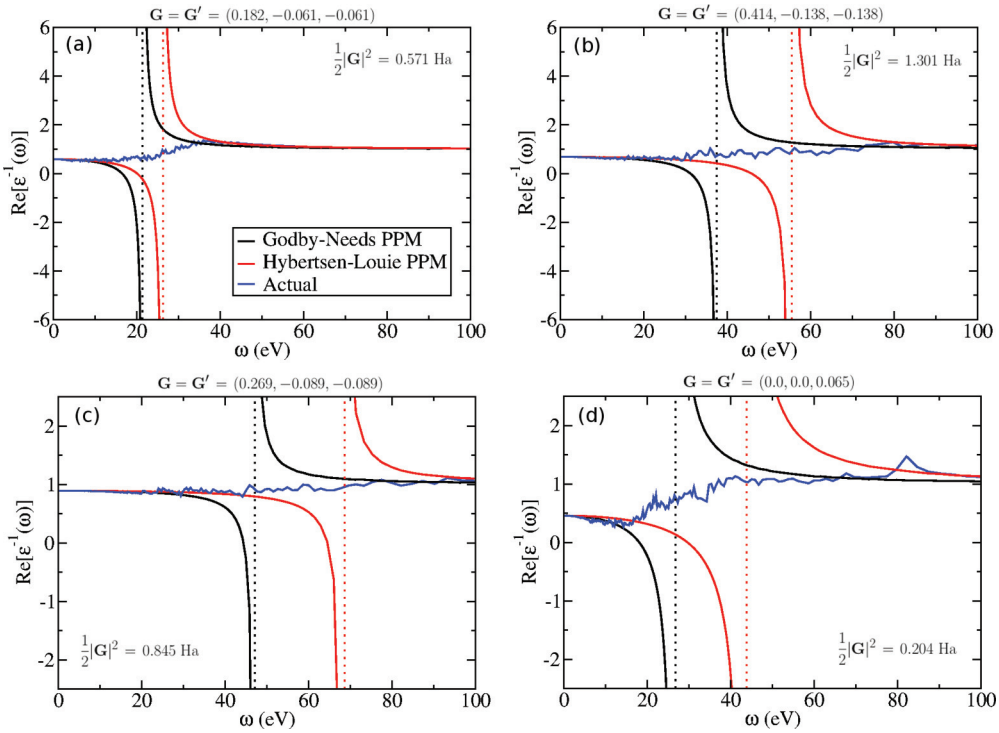

FIG. 6. (Color online) The real part of the inverse dielectric function along the real frequency axis for (a) Si, (b) C, (c) Ne, and (d) ZnO, using the GN and HL PPMs, compared to those obtained from numerical integration. $\mathbf{G} = \mathbf{G}' \neq 0$.

energy levels,[51] largely due to the enforcement of the f-sum rule. The fulfillment of the sum rule is not critical for accurately evaluating the matrix elements of ε^{-1},[51,58] and it is difficult to both satisfy the sum rule and match the overall shape of the dielectric function. The HL, vdLH, and EF PPMs average over a broad range of frequencies, but the weight is concentrated more on the larger frequencies. On the other hand, the GN PPM fits its parameters to two explicitly computed values of ε^{-1} at $\omega = 0$ and $i\omega_p$, leading to good overall match to the actual ε^{-1}, especially in the small-frequency area, which is crucial for evaluating the self-energy Σ for the near-gap states. The summation over a broad range of frequencies diminishes the importance of low-energy excitations, whereas using a single plasma frequency, as in the GN PPM, enhances the importance of the strongly localized states such as the semicore d electrons in ZnO.

The GN PPM agrees not only with the numerical integration very well on E_g, but also on the many-body corrections for individual QP states, as indicated by Table II for the VBM and CBM. In contrast, the HL together with the vdLH and EF PPMs often underestimate ΔE_c while overestimating the magnitude of ΔE_v, though in general, the vdLH and EF PPMs improve over the HL PPM. These results further emphasize that the GN PPM is more reliable than the other three; even in the simple semiconductors such as Si and Ge, it is the error cancellation between ΔE_c and ΔE_v that leads to the calculated E_g using the HL, vdLH, and EF PPMs close to the numerical integration results. But this error cancellation works less well for more localized systems, where the negative shift of E_{VBM} is too large, causing these three PPMs based on the f-sum rule to often overestimate E_g.

IV. SUMMARY AND CONCLUSION

In summary, we conclude that since the accuracy of GW calculation depends on a number of approximations besides the plasmon-pole model, examining the performance of a PPM is complicated. Our results show that even though E_g obtained by the HL PPM agree best with experimental data, the GN PPM best reproduces the electronic screening. In highly delocalized electronic systems the f-sum-rule-based PPMs usually predict very similar E_g to that of the GN PPM due to error cancellation between the band-edge states, whereas in strongly localized systems these three PPMs would dramatically overestimate E_g because the enforcement of the f-sum rule exaggerates electronic screening. But the band-edge energy levels are sensitive to the choice of PPM even in simple semiconductors, in agreement with previous work on the Si/SiO_2 junction,[59] which makes it difficult to accurately determine the energy-level alignment at semiconductor interfaces. The GN model is apparently the most reliable, and the discrepancy between experimental data and the G_0W_0 results cannot be resolved by merely using or building a PPM that happens to offer a correct band gap; instead, better DFT wave functions and eigenenergies, e.g., using LDA/GGA+U,[37,60,61] self-consistent GW[17–21] procedures, and the vertex correction,[19,20] are necessary.

ACKNOWLEDGMENTS

This work was financially supported by a DOE Early Career Award (Grant No. DE-SC0006433). Computations were carried out at the Golden Energy Computing Organization (GECO) at the CSM and National Energy Research Scientific Computing Center (NERSC). Z.W. thanks M. Stankovski for many helpful discussions.

*zhiwu@mines.edu

[1] P. Hohenberg and W. Kohn, Phys. Rev. **136**, B864 (1964).
[2] W. Kohn and L. J. Sham, Phys. Rev. **140**, A1133 (1965).
[3] M. S. Hybertsen and S. G. Louie, Phys. Rev. B **34**, 5390 (1986).
[4] F. Arasyetiawan and O. Gunnarsson, Rep. Prog. Phys. **61**, 237 (1998).
[5] W. G. Aulbur, L. Jonsson, and J. W. Wilkins, Solid State Phys. **54**, 1 (2000).
[6] G. Onida, L. Reining, and A. Rubio, Rev. Mod. Phys. **74**, 601 (2002).
[7] J. P. Perdew, R. G. Parr, M. Levy, and J. L. Balduz, Phys. Rev. Lett. **49**, 1691 (1982).
[8] J. P. Perdew and M. Levy, Phys. Rev. Lett. **51**, 1884 (1983).
[9] L. J. Sham and M. Schlüter, Phys. Rev. Lett. **51**, 1888 (1983).
[10] E. J. Baerends and O. V. Gritsenko, J. Chem. Phys. **123**, 062202 (2005).
[11] S. Kümmel and L. Kronik, Rev. Mod. Phys. **80**, 3 (2008).
[12] A. D. Becke, J. Chem. Phys. **98**, 1372 (1993).
[13] J. P. Perdew, M. Ernzerhof, and K. Burke, J. Chem. Phys. **105**, 9982 (1996).
[14] J. Muscat, A. Wander, and N. M. Harrison, Chem. Phys. Lett. **342**, 397 (2001).
[15] L. Hedin, Phys. Rev. **139**, A796 (1965).
[16] A. L. Fetter and J. D. Walecka, *Quantum Theory of Many-Particle Systems* (McGraw-Hill, New York, 1971).
[17] M. van Schilfgaarde, T. Kotani, and S. V. Faleev, Phys. Rev. Lett. **96**, 226402 (2006).
[18] F. Bruneval, N. Vast, and L. Reining, Phys. Rev. B **74**, 045102 (2006).
[19] M. Shishkin, M. Marsman, and G. Kresse, Phys. Rev. Lett. **99**, 246403 (2007).
[20] M. Shishkin and G. Kresse, Phys. Rev. B **75**, 235102 (2007).
[21] T. Kotani, M. van Schilfgaarde, and S. V. Faleev, Phys. Rev. B **76**, 165106 (2007).
[22] M. S. Hybertsen and S. G. Louie, Phys. Rev. Lett. **55**, 1418 (1985).
[23] X.-Z. Li, R. Gomez-Abal, H. Jiang, C. Ambrosch-Draxl, and M. Scheffler, New J. Phys. **14**, 023006 (2012).
[24] W. Luo, S. Ismail-Beigi, M. L. Cohen, and S. G. Louie, Phy. Rev. B **66**, 195215 (2002).
[25] M. van Schilfgaarde, T. Kotani, and S. V. Faleev, Phys. Rev. B **74**, 245125 (2006).
[26] F. Tran and P. Blaha, Phys. Rev. Lett. **102**, 226401 (2009).
[27] B. I. Lundqvist, Phys. Kondens. Mater. **6**, 193 (1967).
[28] B. I. Lundqvist, Phys. Kondens. Mater. **6**, 206 (1967).
[29] L. Hedin and S. Lundqvist, in *Solid State Physics*, edited by H. Ehrenreich, F. Seitz, and D. Turnbull (Academic, New York, 1969), Vol. 23, p. 1.
[30] A. W. Overhauser, Phys. Rev. B **3**, 1888 (1971).
[31] R. W. Godby and R. J. Needs, Phys. Rev. Lett. **62**, 1169 (1989).

[32] A. Oschlies, R. W. Godby, and R. J. Needs, Phys. Rev. B **51**, 1527 (1995).
[33] W. von der Linden and P. Horsch, Phys. Rev. B **37**, 8351 (1988).
[34] G. E. Engel and B. Farid, Phys. Rev. B **47**, 15931 (1993).
[35] M. L. Tiago, S. Ismail-Beigi, and S. G. Louie, Phys. Rev. B **69**, 125212 (2004).
[36] A. Fleszar and W. Hanke, Phys. Rev. B **71**, 045207 (2005).
[37] B.-C. Shih, Y. Xue, P. Zhang, M. L. Cohen, and S. G. Louie, Phys. Rev. Lett **105**, 146401 (2010).
[38] X. Gonze, B. Amadon, P.-M. Anglade, J.-M. Beuken, F. Bottin, P. Boulanger, F. Bruneval, D. Caliste, R. Caracas, M. Cote, T. Deutsch, L. Genovese, Ph. Ghosez, M. Giantomassi, S. Goedecker, D. R. Hamann, P. Hermet, F. Jollet, G. Jomard, S. Leroux, M. Mancini, S. Mazevet, M. J. T. Oliveira, G. Onida, Y. Pouillon, T. Rangel, G.-M. Rignanese, D. Sangalli, R. Shaltaf, M. Torrent, M. J. Verstraete, G. Zerah, and J. W. Zwanziger, Comput. Phys. Commun. **180**, 2582 (2009).
[39] S. Lebègue, B. Arnaud, M. Alouani, and P. E. Bloechl, Phys. Rev. B **67**, 155208 (2003).
[40] M. Giantomassi, M. Stankovski, R. Shaltaf, M. Grüning, F. Bruneval, P. Rinke, and G.-M. Rignanese, Phys. Status Solidi B **248**, 275 (2011).
[41] M. Cardona and M. L. W. Thewalt, Rev. Mod. Phys. **77**, 1173 (2005).
[42] F. Giustino, S. G. Louie, and M. L. Cohen, Phys. Rev. Lett. **105**, 265501 (2010).
[43] K. J. Chang and M. L. Cohen, Phys. Rev. B **34**, 4552 (1986).
[44] I. Vurgaftman, J. R. Meyer, and L. R. Ram-Mohan, J. Appl. Phys. **89**, 5815 (2001).
[45] F. J. Manjon, M. Mollar, M. A. Hernandez-Fenollosa, B. Mari, R. Lauck, and M. Cardona, Solid State Commun. **128**, 35 (2003).
[46] M. A. Dong-Ping and C. Ju-Rong, Commun. Theor. Phys. **43**, 529 (2005).
[47] T. Miyake, P. Zhang, M. L. Cohen, and S. G. Louie, Phys. Rev. B **74**, 245213 (2006).
[48] C. Friedrich, M. C. Muller, and S. Blugel, Phys. Rev. B **83**, 081101 (2011).
[49] H. Dixit, R. Saniz, D. Lamoen, and B. Partoens, Comput. Phys. Commun. **182**, 2029 (2011).
[50] J. A. Berger, L. Reining, and F. Sottile, Phys. Rev. B **85**, 085126 (2012).
[51] M. Stankovski, G. Antonius, D. Waroquiers, A. Miglio, H. Dixit, K. Sankaran, M. Giantomassi, X. Gonze, M. Cote, and G.-M. Rignanese, Phys. Rev. B **84**, 241201 (2011).
[52] N. Marzari and D. Vanderbilt, Phys. Rev. B **56**, 12847 (1997).
[53] M. Dvorak, S.-H. Wei, and Z. Wu, Phys. Rev. Lett. **110**, 016402 (2013).
[54] A. A. Mostofi, J. R. Yates, Y.-S. Lee, I. Souza, D. Vanderbilt, and N. Marzari, Comput. Phys. Commun. **178**, 685 (2008).
[55] D. L. Johnson, Phys. Rev. B **9**, 4475 (1974).
[56] M. Taut, J. Phys. C **18**, 2677 (1985).
[57] S. B. Zhang, D. Tománek, M. L. Cohen, S. G. Louie, and M. S. Hybertsen, Phys. Rev. B **40**, 3162 (1989).
[58] A. Miglio, D. Waroquiers, G. Antonius, M. Giantomassi, M. Stankovski, M. Cote, X. Gonze, and G.-M. Rignanese, Eur. Phys. J. B **85**, 322 (2012).
[59] R. Shaltaf, G.-M. Rignanese, X. Gonze, F. Giustino, and A. Pasquarello, Phys. Rev. Lett. **100**, 186401 (2008).
[60] V. I. Anisimov, J. Zaanen, and O. K. Andersen, Phys. Rev. B **44**, 943 (1991).
[61] A. I. Liechtenstein, V. I. Anisimov, and J. Zaanen, Phys. Rev. B **52**, R5467 (1995).